Hindawi
Advances in Civil Engineering
Volume 2021, Article ID 5453764, 17 pages
https://doi.org/10.1155/2021/5453764

Research Article

Stability of a Rock Tunnel Passing through Talus-Like Formations: A Case Study in Southwestern China

Shaoqiang Zhang,[1] Wenqiang Li,[1] Jiashan Tan,[1] Bokuan Li,[1] Xiaochang Li,[2] Shuaifeng Wang,[2] and Zixin Zhang[2,3]

[1]*PowerChina Roadbridge Group Co., Ltd., Beijing 100048, China*
[2]*Department of Geotechnical Engineering, College of Civil Engineering, Tongji University, Shanghai 200092, China*
[3]*Key Laboratory of Geotechnical Engineering, Ministry of Education, Tongji University, Shanghai 200092, China*

Correspondence should be addressed to Shuaifeng Wang; 1410264@tongji.edu.cn

Received 9 June 2021; Revised 1 July 2021; Accepted 8 July 2021; Published 24 July 2021

Academic Editor: Guowen Xu

Tayi tunnel is one of the component tunnels in the Jian-Ge-Yuan Highway Project located in Yunnan Province, southeast of China. It mainly passes through talus-like formations comprised of rock blocks of diverse sizes and weak interlayers with clayey soils with different fractions. Such a special composition leads to the loose and fractured structure of talus-like formations, which is highly sensitive to the excavation perturbation. Therefore, Tayi tunnel has become the controlled pot of the whole highway project as the construction speed has to be slowed down to reduce the deformation of surrounding talus-like rock mass. To better understand the tunnel-induced ground response and the interaction between the surrounding rock mass and tunnel lining, a comprehensive in situ monitoring program was set up. The in situ monitoring contents included the surrounding rock pressure on the primary lining, the primary lining deformation, and the stress of steel arches. Based on the monitoring data, the temporal and the long-term spatial characteristics of mechanical behavior of surrounding rock mass and lining structure due to the excavation process were analyzed and discussed. It is found that the excavation of lower benches released the surrounding rock pressure around upper benches, resulting in the decrease of the surrounding rock pressure on the primary lining and the stress of steel arches. In addition, the monitoring data revealed that the primary lining sustained bias pressure from the surrounding rock mass, which thereby caused unsymmetrical deformation of the primary lining, in accordance with the monitored displacement data. A dynamically adaptive support system was implemented to strengthen the bearing capacity of the lining system especially in the region of an extremely weak rock mass. After such treatment, the deformation of the primary lining has been well controlled and the construction speed has been considerably enhanced.

1. Introduction

Southwestern China has a complex terrain and complicated geological conditions with crisscrossed mountains and rivers, inducing complex geotechnical formations such as round gravel and mudstone mixture [1], layered phyllite strata [2], and rock-soil mixtures [3]. The talus-like rock masses, widely distributed in Yunnan Province in western China, are a special kind of geotechnical mixture, which is distinguishingly different from the common rocks, soils, or rock-soil mixture. The talus-like rock masses are mainly distributed in the elurium, colluvium, and diluvial layers of Quaternary System. The main components of the talus-like rock masses are rock blocks with diverse sizes with interlayers filled with weak rock or clayey soils with different fractions, which can be regarded as special weak rock masses. Different from the traditional rock-soil mixture, the talus-like formations are a special kind of geotechnical mixture and have very complicated compositions with a wide range of grain diameters.

The recent studies about geotechnical mixture are mainly focused on the traditional talus development [4, 5]

and the rock-soil mixture [6–10] including in situ survey and laboratory test. Coli et al. [11] carried out an in situ shear test on shale-limestone chaotic complex bimrock and calculated its strength parameters based on a limit equilibrium analysis. Afterwards, the possible correlations between the scarce direct information from the in situ shear test data and the large indirect information from the synthetic image parameters were presented based on geostatistics [12]. Xu et al. [13] obtained the rock proportion and the granular distribution of soil-rock mixture using a combined method with large-scale direct shear test and digital image analysis, which was then implemented to investigate the mixture's shear strength characteristics and failure mechanism. Kalender et al. [14] developed a preliminary empirical strength criterion for determining the strength parameters of an unwelded rock-soil mixture by considering the mechanical behavior of the boundaries between matrix and blocks based on in situ and lab tests data. Afifipour and Moarefvand [15] conducted a series of uniaxial compression tests on artificial bimrocks models with high rock block proportions to investigate the bimrocks' mechanical behavior. In addition to the physical tests, the numerical simulation is also a mighty approach to investigate the mechanical and failure mechanisms of rock-soil mixture. Tsesarsky et al. [16] presented the influences of volumetric block proportion, block shape, and block orientation on the elastic moduli using finite element simulation. Xu et al. [17] developed a new multi-circle representation method of random polygonal blocks to generate the mesostructure model of a rock-soil mixture and implemented the model into simulating the mechanical behaviors of rock-soil mixture. Meng et al. [18] presented a numerical study on the elastic property of a rock-soil mixture using random mesostructure generation and found that the elastic modulus decreases gradually with an increase in the model size. Khorasani et al. [19] derived an equation linking the safety factor of bimslope (a slope formed by bimrocks) with volumetric block proportion using physical tests and corresponding numerical simulations, making it possible to evaluate the range of safety factors based on volumetric block proportion. Although there are series of studies on rock-soil mixtures and talus formations, there are still no guides or criteria especially for the talus-like formations, which brings uncertainty and hidden danger to the supporting structure design of tunnels and slopes excavated in such type of rock mass.

This paper investigates the stability of a tunnel passing through talus-like rock masses via site survey and field monitoring. Firstly, the paper describes the basic information about the project case. In the project, the in situ monitoring items included the pressure on the primary lining from the surrounding rock mass, the stress of steel arches, and the deformation of the primary lining. Afterwards, the influence of construction activities on the talus-like ground and the stability characteristics of the tunnel in talus-like rock masses are analyzed based on in situ monitoring. Finally, a dynamically adaptive support system is presented based on the mechanical characteristics of talus-like formations.

2. Project Background

2.1. Project Overview. The Jian-Ge-Yuan Highway Project is located in the southern Yunnan Province, linking up the Jianshui County, Gejiu City, and Yuanyang County, as shown in Figure 1. The length of the project is about 124.5 km, with 100 bridges and 29 tunnels. The length of bridges and tunnels occupies 72% of the total length of the project. Tayi tunnel, one of the component tunnels in the Jian-Ge-Yuan Highway Project, is located at the junction of Jianshui County and Yuanyang County, as shown in Figure 1(b). There are two lines in the tunnel: the left line is 2616 m long (from Z5K62 + 502 to Z5K65 + 118) and the right line is 2593 m long (from K62 + 489 to K65 + 082). The buried depth mainly ranges from 100 m to 250 m with a maximum depth of 297 m.

2.2. Geological Conditions. Tayi tunnel passes across Red River fault zone, resulting in developed secondary structures and complex lithology due to the rupturing movement. The tunnel mainly passes through moderately to strongly weathered slate mixed up with siltstone, limestone, mudstone, and soil. Dense fractures and minor structures in the rock mass are heavily developed with sharply steep dip angles and disordered dip directions. The development of weak bands with irregular distribution brings up fragmented and loose rock masses with poor integrity, inducing a low ability of self-stabilization of the excavated tunnel.

Up to now, 10 boreholes have been conducted to explore the geological conditions along the tunnel route, the detailed information of which is listed in Table 1. The encountered rock mass was evaluated according to the Chinese standard for engineering classification of rock masses [20] and code for design of road tunnels [21]. In general, the rock mass can be divided into different categories ranging from grade I to grade V based on the hardness degree, intactness index, and the quantitatively basic quality index BQ. The BQ value is obtained as

$$\mathrm{BQ} = 90 - 3R_C + 250K_V, \tag{1}$$

where R_C is the uniaxial compressive strength of the rock mass and K_V is the intactness index of the rock mass. The higher the grade is, the more fragmented and weathered the rock mass will be. In Tayi tunnel, grade IV rock mass accounts for about 30%, and grade V covers about 70% of the route. The revealed rock mass in the boreholes is shown in Figure 2, where the range of tunnel section indicates the values of depth of tunnel vault and invert, respectively. It should be noted that the given range of the tunnel section is usually larger than the actual excavation height of the tunnel (Figure 2).

The surrounding rock masses exhibit an obvious characteristic of hybrid formation composited by rock and weak interlayer filled with soil or other weaker rock as shown in Figure 2. Figure 3 gives some examples revealed during the tunnel excavation showing the complex formation. At chainage Z5K62 + 936 of the left line, the rock mass is composited by slate and weak interlayer filled with

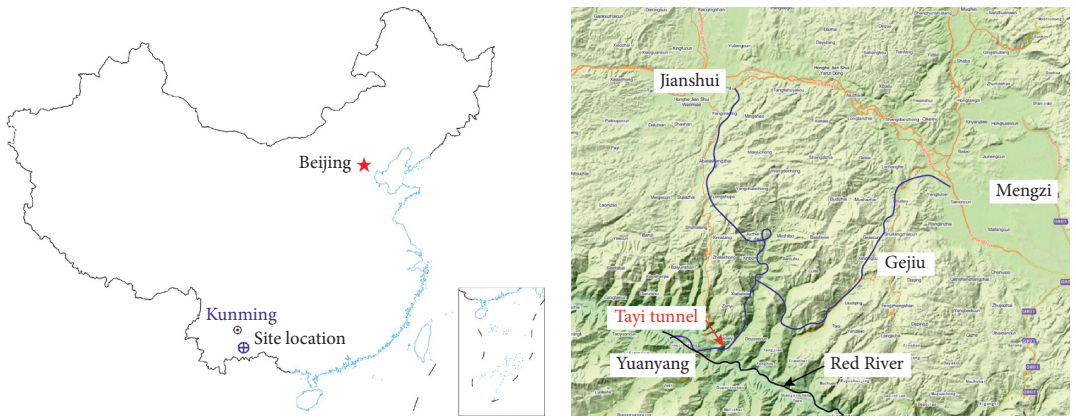

(a) (b)

Figure 1: Site location (a) and layout plan (b) of the Jian-Ge-Yuan Highway Project. The site location is based on the standard map (no. GS(2019) 1684) by Ministry of Natural Resources of the People's Republic of China. The layout plan is based on the online map by National Platform for Common Geospatial Information Services of the People's Republic of China.

mudstone and has a highly loose and fragile structure with low strength (Figure 3(a)), which can be easily crushed by hand. Figures 3(b) and 3(c) show a type of fractured slate sandwiched by clay soil and a mixed rock mass formed by slate, limestone, and carbonaceous mudstone at Z5K63 + 966 and Z5K64 + 455, respectively. In the right line, twisted layers composited by slate and limestone, isolated rock blocks cut by weak mudstone interlayers, and limestone with carbonaceous mudstone interlayer were explored at K62 + 860, K64 + 530, and K64 + 570, as shown in Figures 3(d)–3(f), respectively. The abovementioned geological mixture composited by rock and soil (or weaker rock) revealed in Tayi tunnel is quite different from the traditional rock-soil mixture (often called talus formation) as explored by previous studies [17, 22–24], which can be regarded as rock-in-soil talus. Thus, we tentatively call such a kind of rock masses composited by rock and soil as talus-like formations. They are sensitive to the excavation perturbation, inducing that Tayi tunnel has become the controlled pot of the whole highway project as the construction speed has to be slowed down in order to reduce the deformation of surrounding talus-like ground. The explored engineering problems in the tunnel include (1) large deformation of the primary lining (Figure 4(a)), (2) rock collapse of the excavation surface and side walls (Figures 4(b) and 4(c)), and (3) broken primary lining (Figure 4(d)).

2.3. Construction Design and Support System. Tayi tunnel is constructed using the bench cut method with three steps as shown in Figure 5. The heights of the three benches are 3.98 m, 3.76 m, and 2.86 m from the top-down, respectively (Figure 5(b)). Usually, the length of the upper bench is about 8 m to ensure enough space for the operation of excavation machinery. The excavated tunnel is designed to be supported by a compound primary lining composited by mortar anchors, steel meshes, I-beam steel arches (Figure 5(c)), and shotcrete. After the installation of steel arches of each bench, two-foot reinforcement bolts (42 mm radius and 3.5 m length) are used on both sides to strengthen the bearing capacity of steel arches (Figure 5(a)). As shown in Figure 5(b), the spacing along the excavation direction of steel arches is 80 cm and thus the longitudinal spacing of mortar anchors is set as 80 cm, while the circumambient spacing is 120 cm. According to the longitudinal spacing of steel arches, the length of each excavation step of the upper bench is set as 1.6 m and the excavation length of middle and lower benches is set as 2.4 m, i.e., two and three times of the spacing, respectively. The secondary lining is in the form of cast-in situ reinforced concrete with 45 cm thickness, of which the reinforcement design is shown in Figure 5(d). The reserved deformation between the primary and second linings is 10 cm. Before excavation of the upper bench, grouting tremies with 42 mm radius, 3.5 mm thickness, and 4.5 m length are used to pre-support the surrounding rock masses. The longitudinal spacing of the tremies is 80 cm to match the installation of steel arches and the circumambient is 30 cm. The inclination angle to pipe the tremies is set as 40° to ensure the splicing length between two adjacent tremies is larger than 3.9 m. It should be noted that this system support is designed for the general grade IV~V surrounding rock masses.

3. Insight from the In Situ Monitoring

To investigate the mechanical characteristics of the primary lining in talus-like rock masses, in situ monitoring was established in Tayi tunnel, including the pressure on the primary lining from surrounding rock, the stress of steel arches, and the deformation of the primary lining.

3.1. Monitoring Scheme. The deformation of the primary lining was measured by the total station. There were 5 monitoring points in each monitoring section as shown in Figure 6(a), which were mainly located on the upper bench. The monitoring points were established after spraying the shotcrete of the primary lining. The primary

Table 1: Detailed information of boreholes.

Borehole no.	Chainage (left line)	Chainage (right line)	Depth of borehole (m)	Range of tunnel section (m)	[BQ]	Grade
BH-01	—	K62 + 875	80.69	72.34~80.69	265	IV ~ V
BH-02	Z5K63 + 396.4	K63 + 375.64	145.01	126.13~145.01	215	V
BH-03	Z5K63 + 620.67	K63 + 597	141.7	128.8~141.7	92.5	V
BH-04	—	K63 + 643	153.5	140~153.5	105	V
BH-05	Z5K63 + 769.3	K63 + 753	200.6	185.2~200.6	272	IV
BH-06	Z5K63 + 842.65	K63 + 817.7	209.5	195~209.5	255	IV ~ V
BH-07	Z5K63 + 954.91	K63 + 930	255.2	233.5~255.2	312	IV
BH-08	Z5K64 + 180.23	K64 + 156.45	305	278.7~300.1	275	IV
BH-09	Z5K64 + 310.46	K64 + 286	305.3	283~305.3	267	IV ~ V
BH-10	—	K64 + 700	213.67	193.08~213.67	265	IV ~ V

Note: [BQ] is the estimated BQ value according to the geological conditions of boreholes.

Figure 2: Pictures for the revealed rock mass by boreholes.

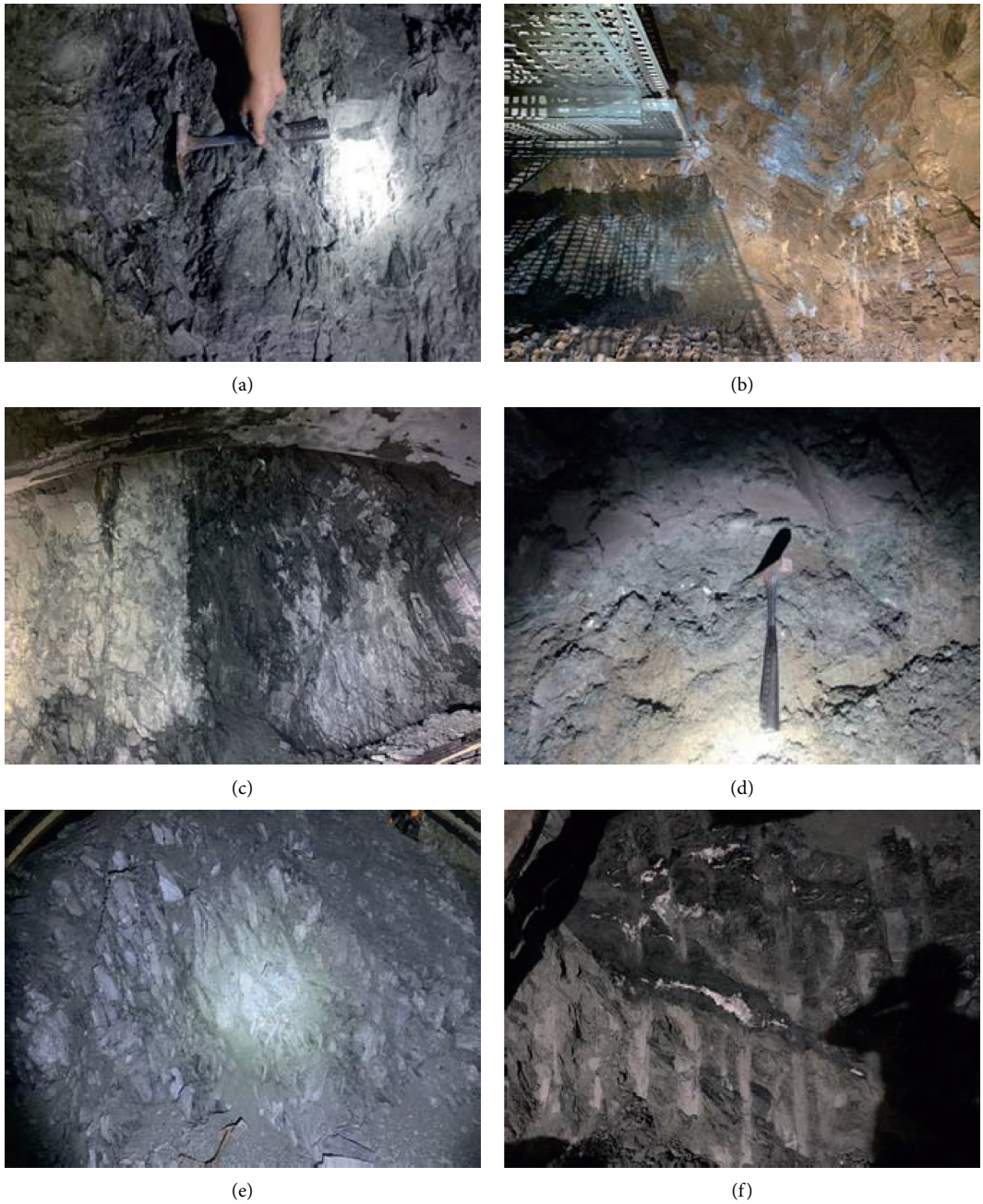

Figure 3: Talus-like rock mass encountered during the tunnel excavation: (a) slate and weak interlayer filled with mudstone at Z5K62 + 936; (b) slate and weak interlayer filled with weathered rock and soft soil at Z5K63 + 966; (c) mixture of slate, limestone, and carbonaceous mudstone at Z5K64 + 455; (d) twisted layers composited by slate and limestone at K62 + 860; (e) isolated rock blocks cut by interlayers filled with weak mudstone at K64 + 530; (f) limestone with carbonaceous mudstone interlayer at K64 + 570.

lining deformation was carried out every 5 m along the tunneling direction and measured twice a day. 7 monitoring points are designed to measure the pressure on the primary lining from surrounding rock and the stress of steel arches as shown in Figure 6(b). The pressure on the primary lining from surrounding rock was measured by vibrating wire pressure transducers, which were located on the outer surface of steel arches (Figures 6(b) and 7). The stress of steel arches was monitored by vibrating wire stress transducers, which were located in the junction of the web and flanges of the steel I-beam as shown in Figures 6(b) and 7. These transducers were fixed after the location of steel arches and before spraying shotcrete. Two monitoring sections in the left line, i.e., Z5K64 + 500 and Z5K64 + 540, were chosen to obtain the surrounding rock pressure and steel arch stress, which were measured once a day. The measurement items are summarized in Table 2. It should be noted that the tunnel was excavated from a larger to a smaller value of chainage, i.e., from Z5K64 + 540 to Z5K64 + 500.

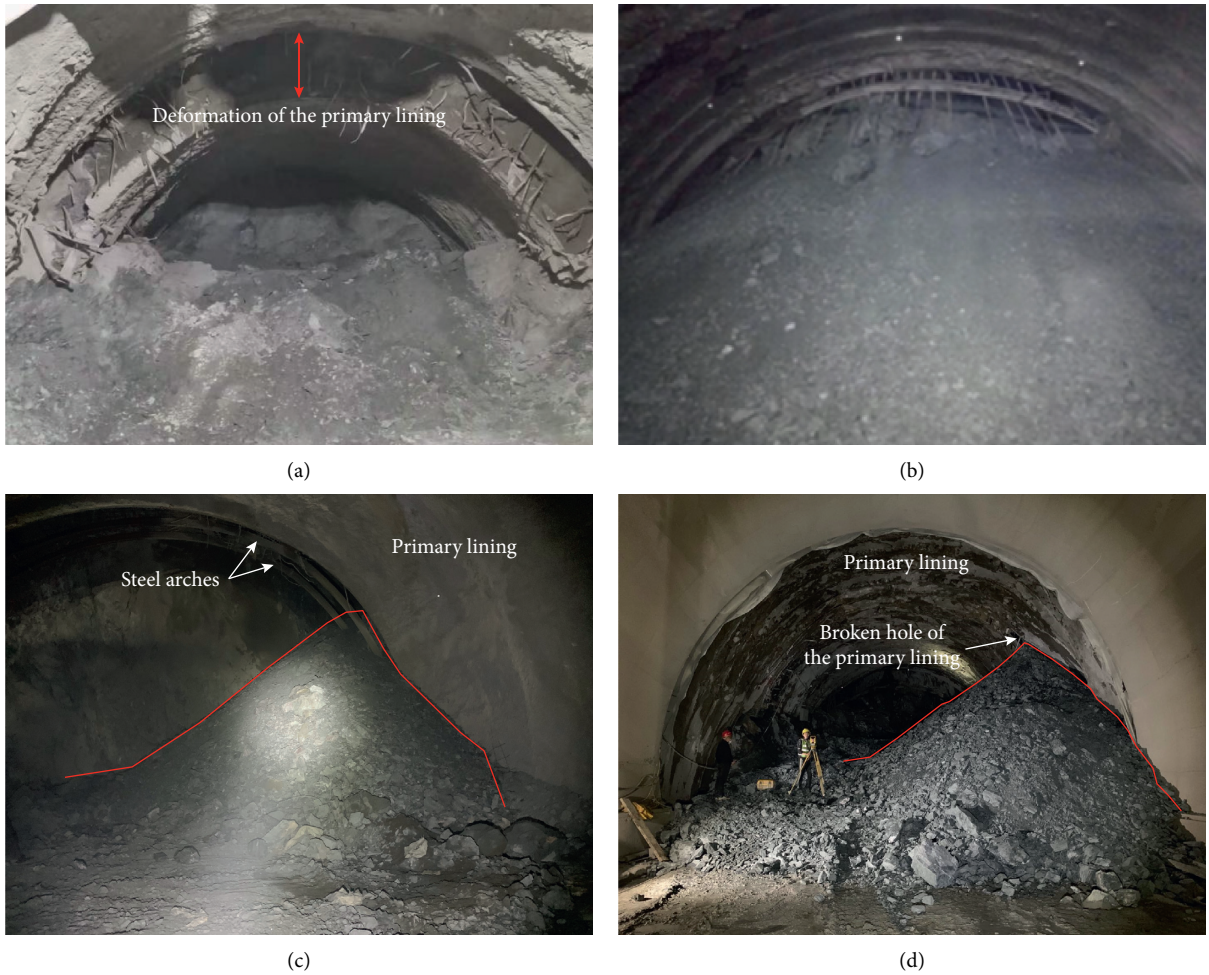

Figure 4: Engineering problems in Tayi tunnel: (a) large deformation of the primary lining due to soft surrounding rock mass; (b) collapse of the tunnel excavation face; (c) collapse of the tunnel side wall after installing steel arches but before spraying shotcrete of the primary lining; (d) broken primary lining after spraying shotcrete.

3.2. Results and Analysis

3.2.1. Deformation of Primary Lining

(1) Influence of Construction Activities on Primary Lining. Tayi tunnel was shut down from the noon of September 19th in 2020 to the morning of September 24th in 2020 due to scheduled maintenance of large-scale mechanical equipment. Therefore, it is reasonable to regard the duration from September 20th to 23rd as downtime, when the chainage of the excavation face was Z5K64 + 576.6. The monitoring data from September 11th to 28th were selected to show the deformation of the primary lining before, during, and after the downtime. Taking Z5K64 + 600 as an example, Figure 8 illustrates the displacements of five monitoring points (as shown in Figure 6). The diurnal displacement of the primary lining during the downtime was smaller than the data before and after the downtime, especially from September 21st to 23rd. Figure 9 shows the diurnal displacement of point A at the tunnel vault in chainages from Z5K64 + 610 to Z5K64 + 580, which yields the same rule with Figure 8. It can be concluded that the deformation of primary lining caused by the construction activities, including face excavation, boring, and drilling pipes, is larger than the deformation caused by surrounding rock creep in the talus-like ground. In addition, the construction activities have more impact on the closer sections (Z5K64 + 610 to 600) than the farside sections (Z5K64 + 595 to 580).

(2) Spatial-Temporal Evolution of Primary Lining Deformation. Figure 10 shows the time-history curve of deformation of primary lining at Z5K64 + 500 and Z5K64 + 540. All the monitoring points were measured on the first day when they were located, inducing that the horizontal axis indicated the number of monitoring days and begun from 1. The time-history curves of different monitoring points yield a similar evolution rule: the diurnal displacement increased rapidly soon after the excavation of the upper bench, then dropped down, and finally tended to be a stable small value about 31 days after the excavation of the upper bench; i.e., the total displacement reached a steady value. In general, the excavation of middle and lower benches influenced the deformation of the primary lining in the form of increasing the diurnal displacement at Z5K64 + 500. However, such a

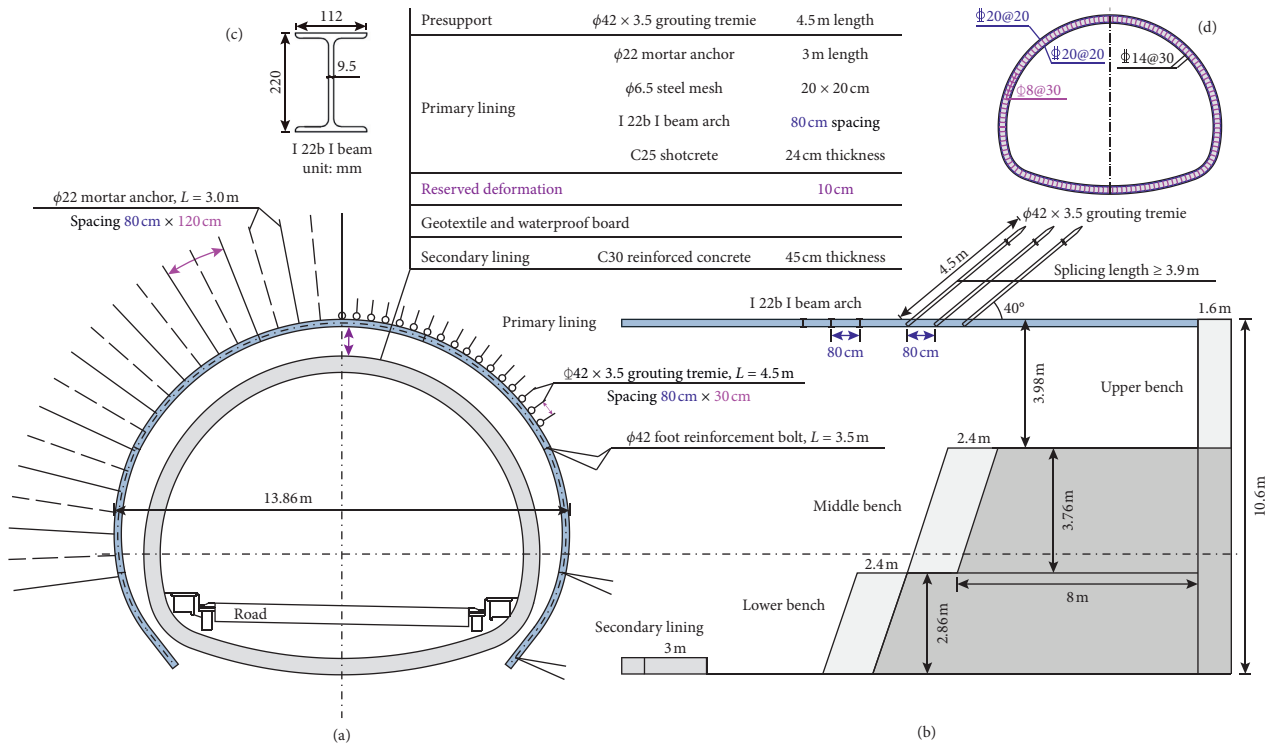

Figure 5: Schematic diagram of construction design for supporting system: (a) cross section; (b) longitudinal section; (c) geometrical information of I 22b I beam; (d) reinforcement design of the secondary lining.

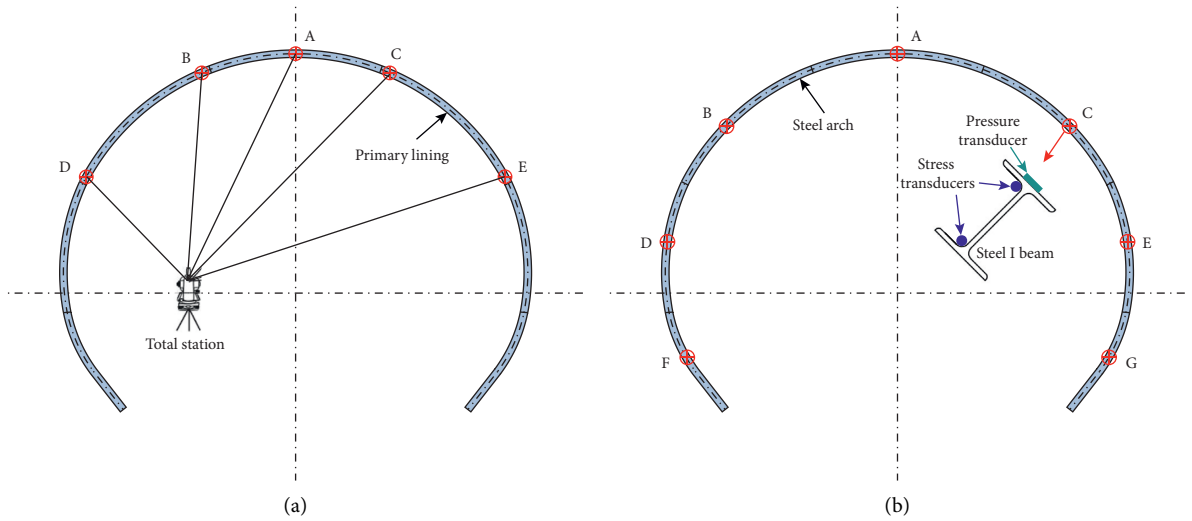

Figure 6: Monitoring points of (a) deformation of the primary lining and (b) surrounding rock pressure and steel arch stress.

phenomenon was not distinct at Z5K64 + 540. In terms of the spatial distribution (Figure 11), the primary lining bore an uneven and asymmetrical deformation at both sections. The maximum total displacement was located at the left or right spandrel of the primary lining while the minimum value happened to the springing.

3.2.2. Surrounding Rock Pressure on Primary Lining. In Figure 12, almost all the monitoring points had positive data; i.e., the force on the primary lining from the surrounding rock is pressure. In consideration of the deformation shown in Figure 10, the surrounding rock shrunk after the excavation, which accords with the rational analysis. It should be noted that points D and G at Z5K64 + 500 had small negative values after the excavation. The reason might be that there was a small gap or void between the primary lining and the surrounding rock induced by the concrete shrinkage, which would cause a small magnitude of tension on the surface of the transducers.

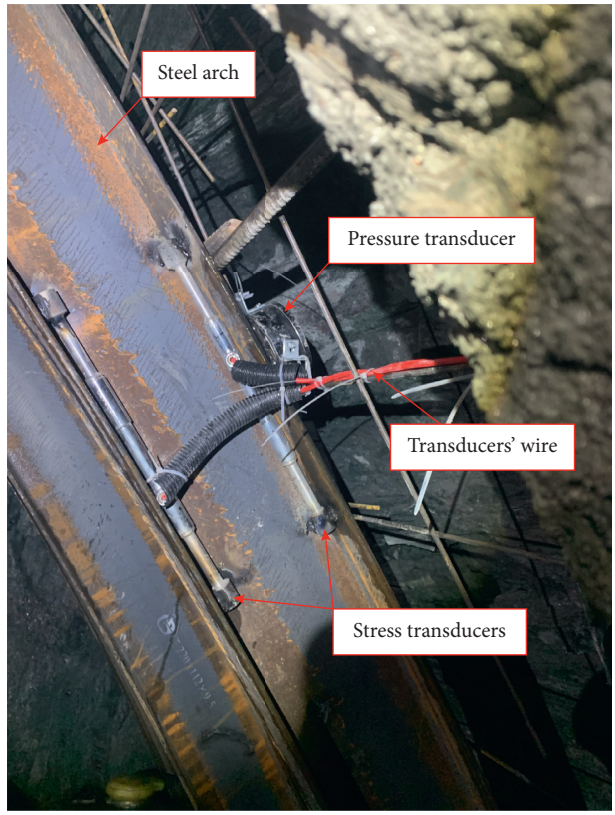

Figure 7: Locations of pressure and stress transducers.

(1) Temporal Evolution of Surrounding Rock Pressure. The surrounding rock pressure on the primary lining increased rapidly in the first 5 days after the excavation of the upper bench as shown in Figures 12(a) and 12(c). Afterwards, the surrounding rock pressure decreased in the subsequent several days. Once the middle bench was excavated, the surrounding rock pressure around the upper bench dropped. Meanwhile, the pressure on the primary lining of the middle bench increased. Similarly, the surrounding rock pressure on the primary lining of the upper and middle benches dropped slightly after the installation of the primary lining of the lower bench. The reason inducing the decrease is that the excavation of lower benches can release some amount of surrounding rock pressure around upper benches. In addition, the excavation of the lower bench had a relatively bigger impact on the surrounding rock pressure on the primary lining of the middle bench than the one of the upper bench. The peak value of the surrounding rock pressure on the primary lining of upper bench appeared 4~6 days after the excavation. As shown in Figures 10(a) and 10(c), the surrounding rock pressure tended to be stable about 35 days after the excavation of the upper bench. Moreover, the steady values decreased from top to bottom, revealing that the upper part of the primary lining bears more surrounding rock pressure than the lower part.

(2) Spatial Evolution of Surrounding Rock Pressure. The spatial distribution of the surrounding rock pressure in Figures 12(b) and 12(d) had an obvious characteristic of discreteness due to coupling factors such as surrounding rock properties, excavation patterns, supporting parameters, and in situ stress level. The peak and steady values at sections Z5K64 + 500 and Z5K64 + 540 were quite different. In general, the deformation at Z5K64 + 540 was larger than the one at Z5K64 + 500 as shown in Figure 12, inducing larger peak and steady values at Z5K64 + 540. According to the site survey, the dominating formations around the two sections were both strongly weathered slate while there was a small interlayer of soft carbonaceous mudstone around Z5K64 + 540, resulting in a worse ground condition at this section. Therefore, the section of Z4K64 + 540 had a larger peak and steady values in surrounding rock pressure.

Influenced by the in situ stresses and uneven excavation of the tunnel periphery, the surrounding rock pressure showed obvious asymmetry. For the primary lining of the upper bench, the pressure on the right was larger than the left in both sections. However, the pressure on the primary lining of the middle and lower benches yielded an opposite rule. The spatial distribution of the surrounding rock pressure along the perimeter of the tunnel also had an obvious characteristic of discreteness. In general, the surrounding rock pressure around the upper part was larger than the lower part.

3.3. Stress of Steel Arches. At each monitoring point, two stress transducers measured the stresses of the outer and inner flanges of the steel I-beam. The actual stress of the steel arch can be calculated by averaging the two values. Figure 13

Table 2: Measurement items for mechanical characteristics of the primary lining.

		Measurement items		
		Surrounding rock pressure	Steel arch stress	Primary lining deformation
Monitoring section	Z5K64 + 500	✓	✓	✓
	Z5K64 + 540	✓	—	✓
	Every 5 m	—	—	✓
Instrument		Vibrating wire pressure transducer	Vibrating wire stress transducer	Total station
Monitoring frequency		1 time/day	1 time/day	2 times/day

Note: the primary lining deformation was measured twice a day at 8 am and 6 pm, whereas the surrounding rock pressure and steel arch stress were measured once a day at 6 pm. Therefore, the monitoring data in the following used the data recorded at 6 pm.

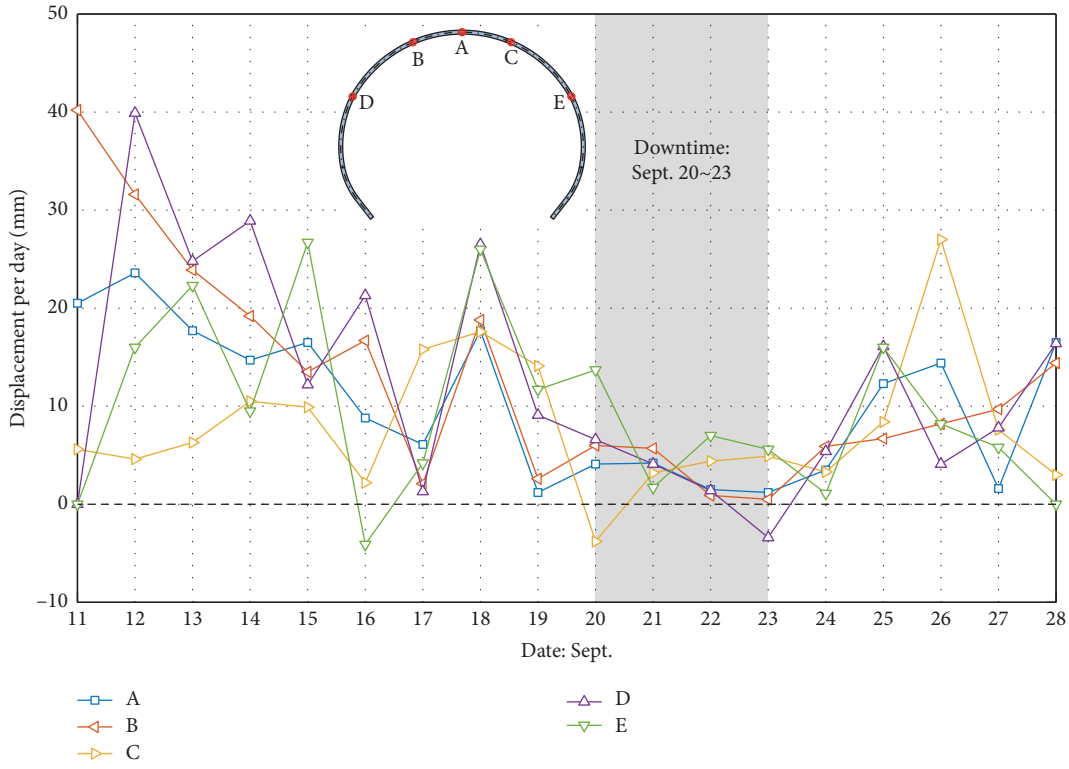

Figure 8: Displacement of monitoring points in chainage Z5K64 + 600 from September 11th to 28th in 2020.

illustrates the stress of steel arches at the section of Z5K64 + 500. Similar to the rules of surrounding rock pressure, the stress of steel arches in the upper bench increased rapidly soon after the excavation, then dropped, and finally tended to be stable. The stress of steel arches at middle and lower benches was less affected by the excavation than the upper bench, which first increased and then tended to be stable. There is no clear descent stage of the data curve of middle and lower benches. The excavation of lower benches released the surrounding rock pressure on the primary lining, inducing the decrease of the force undergone by the primary lining. This phenomenon appeared in the form of the stress decline of the steel arches as shown in Figure 13(a). The stress of steel arches tended to be stable about 40 days after the excavation of the upper bench. Similar to the surrounding rock pressure, the stress of steel arches unevenly distributed along the tunnel periphery (Figure 13(b)). In the upper bench, the stress of steel arches at the tunnel vault was the largest and the right spandrel bore larger stress than the left spandrel. In the stable stage of the data curve, the steady stress decreased from upper benches to lower benches.

4. Control Measures for Tunnel Support in Talus-Like Formations

4.1. Mechanical Characteristics of Talus-Like Formations. Generally, the mechanical characteristics of talus-like rock mass are similar to common weak rock masses [25–30] or layered rock masses [31–33]. However, there are still differences between the two types of rock masses. Firstly, the talus-like rock masses are more affected by the excavation activities than the common weak rock masses. With the bench cut method, the lower benches obviously release the

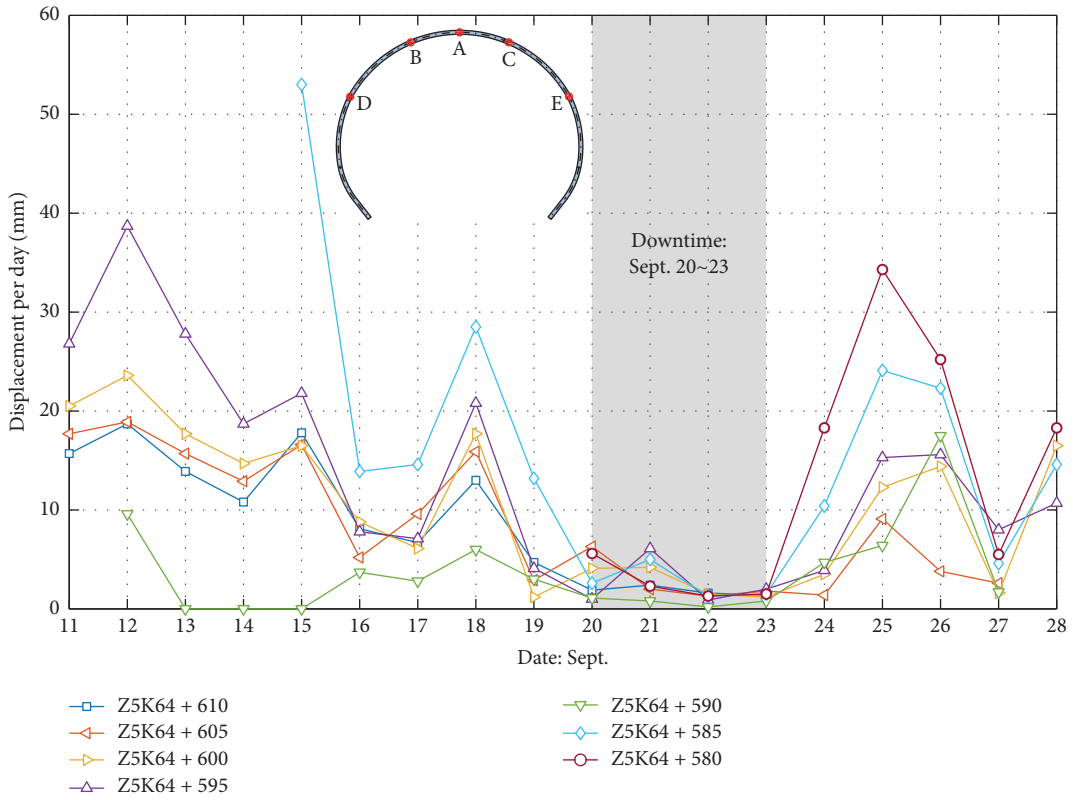

Figure 9: Displacement of point A (tunnel vault) at chainages from Z5K64 + 610 to Z5K64 + 580 during September 11th to 28th in 2020.

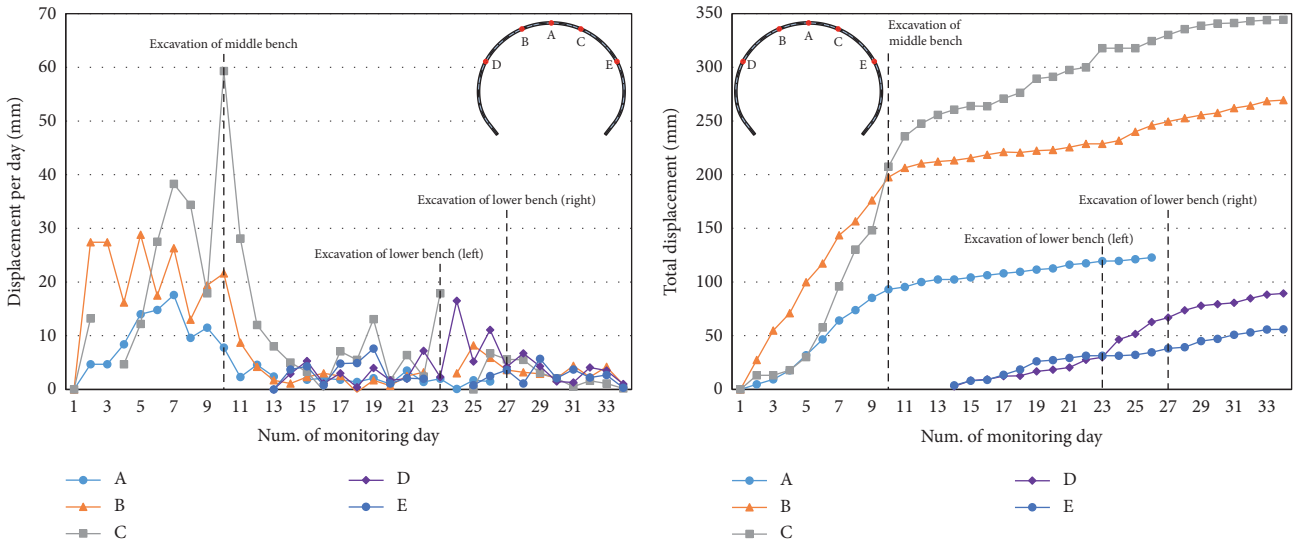

Figure 10: Continued.

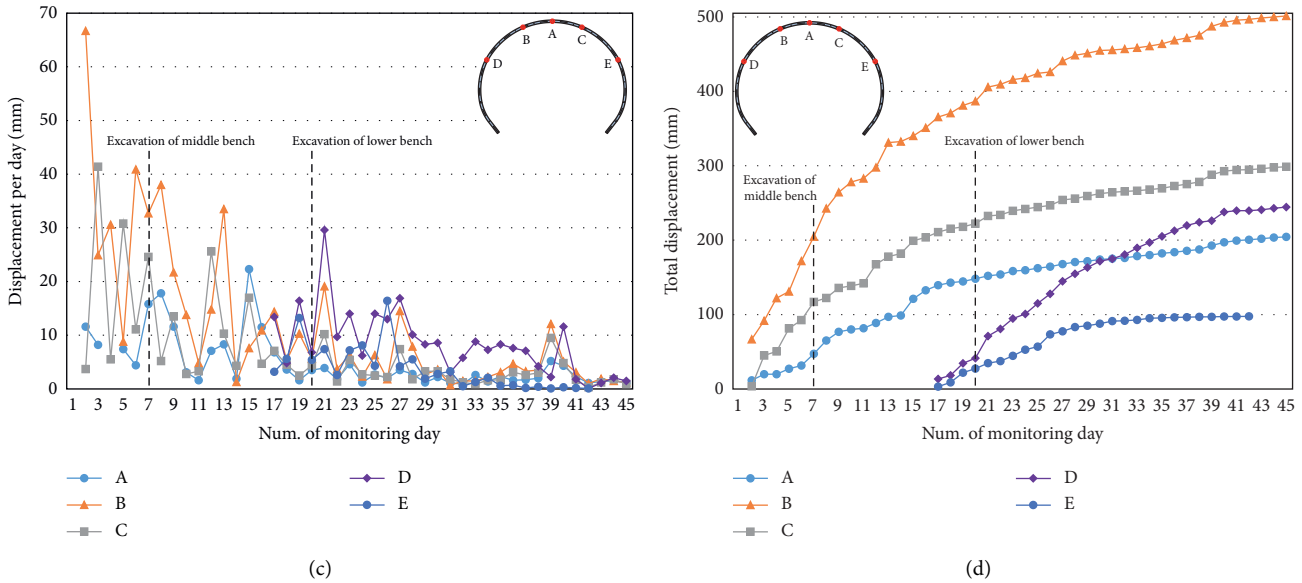

Figure 10: Time-history curve of the deformation of the primary lining: (a) diurnal and (b) accumulative displacement at Z5K64 + 500; (c) diurnal and (d) accumulative displacement at Z5K64 + 540.

surrounding rock pressure around the upper benches, inducing the decline of the surrounding rock pressure on the primary lining and the stress of steel arches. After the installation of the primary lining of the lower benches, the surrounding rock pressure and the stress of steel arches increase slightly and finally tend to be stable. The increasement and speed of the stress of steel arches are larger than the ones of surrounding rock pressure. Secondly, the talus-like rock masses have more complex formations of rock blocks with wide-range sizes and soils with different fractions. Therefore, it is extremely difficult to ensure the evenness of the tunnel periphery during mechanical excavation, which will induce uneven and asymmetrical contact between the surrounding rock mass and the primary lining. As a result, the surrounding rock pressure on the primary lining, the inner stress of the steel arches, and the deformation of the primary lining usually have a characteristic of discreteness and nonuniformity along the tunnel periphery. Accordingly, the evolution of the interaction between the surrounding rock and the primary lining can be concluded into three stages: (1) the deformed surrounding rock mass contacts with the primary lining and exerts sharp pressure on the primary lining, and the deformation of the surrounding rock mass is larger than the one of the primary lining; (2) the interactional pressure between the surrounding rock mass and the primary lining releases and decreases, and the deformation rate of the surrounding rock mass becomes smaller than the one of the primary lining; (3) the surrounding rock pressure tends to be stable and the deformations of the surrounding rock mass and the primary lining become coordinating.

In consideration of the complex formations and weakness of the talus-like formations, the deformation of surrounding rock masses should be emphatically disposed during the tunnel excavation. Termly advanced detection is recommended to obtain the information of rock mass properties ahead of the excavation face, such as the fragmentation degree, the lithological components, and water content. It is also suggested that the forepoling is established in time and changes momentarily if the advanced detection explores a worse rock mass. The invert part should be excavated and installed timely to enclose the primary lining into integrity to ensure the performance of the lining. Moreover, the secondary lining should be installed as soon as possible when the deformation of the primary lining tends to be stable to diminish the exposure duration of the primary lining.

4.2. Dynamically Adaptive Support System in Talus-Like Formations. In consideration of the significant influence of the talus-like formations on the tunnel support system, a reasonable modification of the support system had been processed. Firstly, the talus-like formations, which had been classified into grade V rock mass, were divided into three subclasses according to the ground condition: (1) the extremely weak and fractured rock mass without water inflow as Vd-1; (2) the extremely weak and fractured rock mass with water inflow as Vd-2; (3) the extremely weak and fractured rock mass mixed with some amount of soil and water inflow as Vd-3. It should be noted that the item "Vd" came from the geological investigation report of Tayi tunnel and the letter "d" herein is just a notation showing that such a type of rock mass is weaker and more dangerous than grade V rock mass. Secondly, a dynamically adaptive support system was proposed to adapt to the varying conditions of talus-like formations as shown in Figure 14. The spacing of steel arches was changed to 60 cm and thus the excavation length of the upper bench was altered to 120 cm for grades Vd-1 and Vd-2 rock masses and 60 cm for grade Vd-3 rock

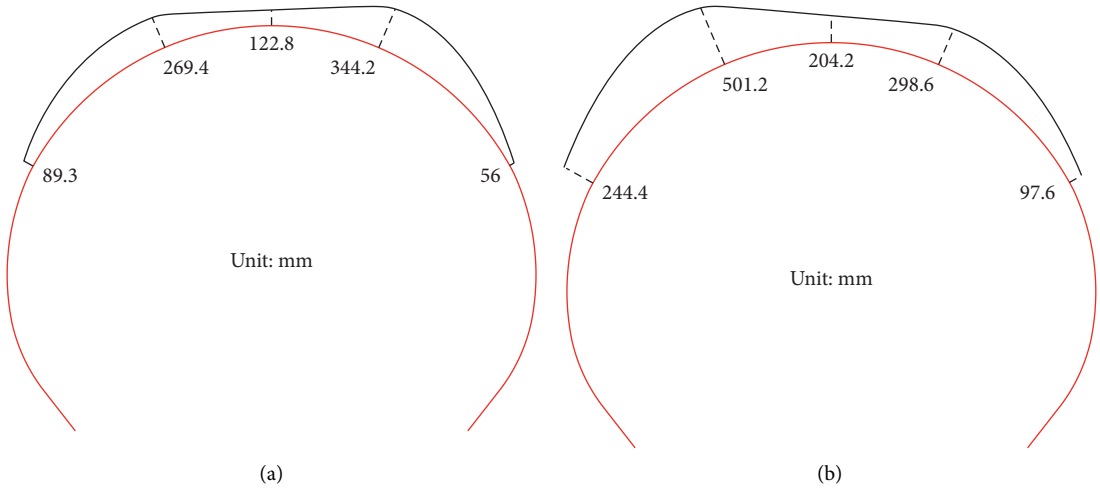

(a) (b)

Figure 11: Spatial distribution of total displacement of the primary lining at (a) Z5K64 + 500 and (b) Z5K64 + 540.

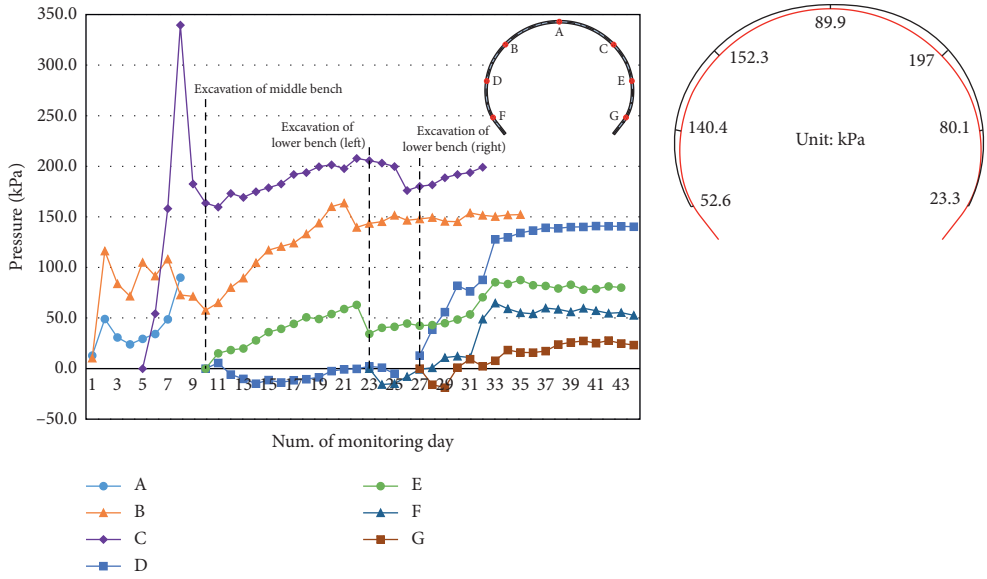

(a) (b)

Figure 12: Continued.

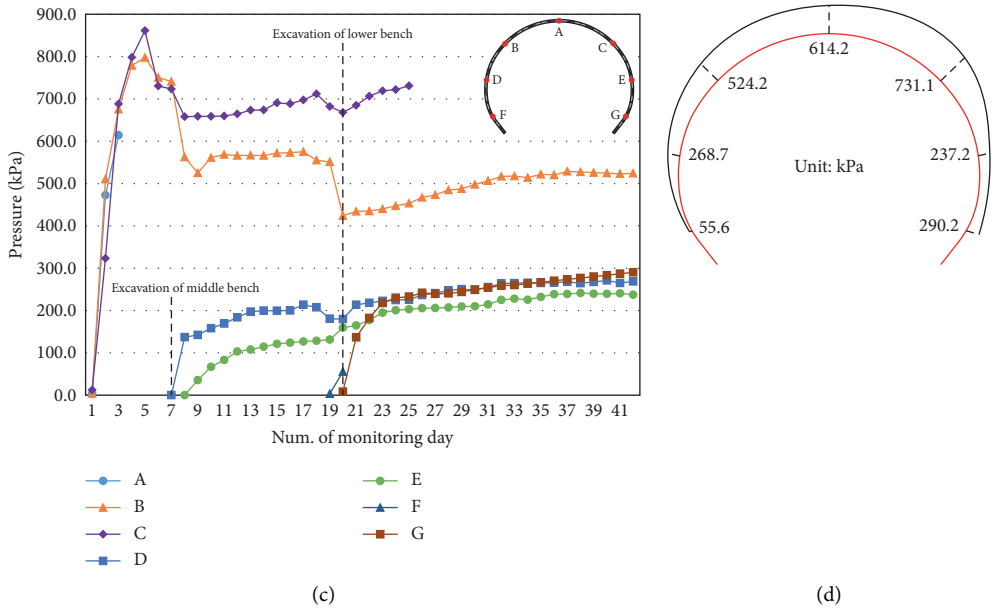

Figure 12: Surrounding rock pressure on the primary lining: (a) time-history curve and (b) spatial distribution at Z5K64 + 500; (c) time-history curve and (d) spatial distribution at Z5K64 + 540. The spatial distribution diagrams were based on the last data of the time-history curve.

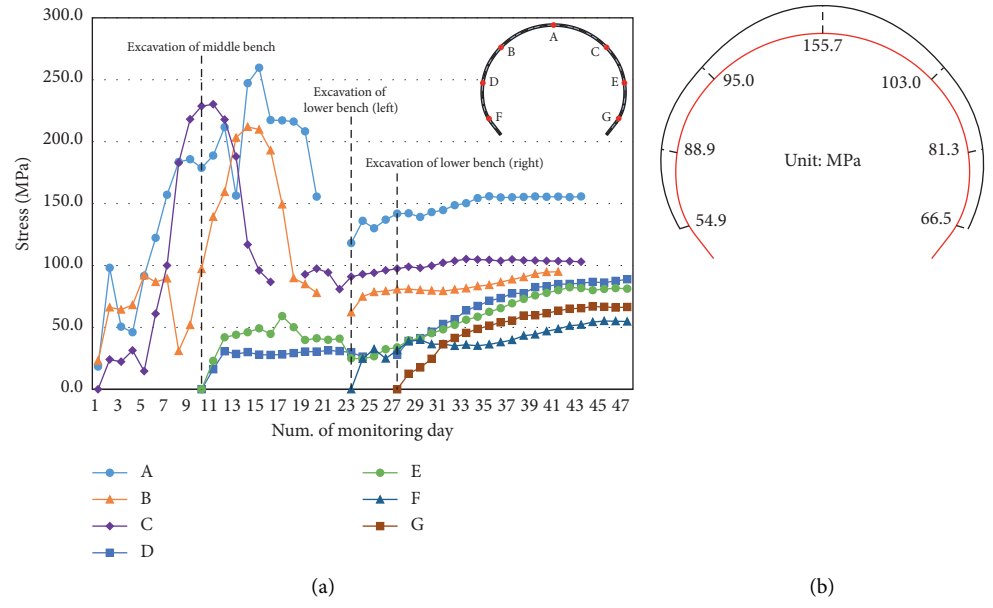

Figure 13: (a) Time-history curve and (b) spatial distribution of steel arch stress at Z5K64 + 500. The spatial distribution diagrams were based on the last data of the time-history curve.

mass, respectively. The excavation length of the middle and lower benches was set as 180 cm, i.e., three times of the steel arch spacing. In the dynamically adaptive support system, the pre-support scheme used pipe shed to prevent the deformation of the surrounding rock mass ahead of the excavation face. As for the primary lining, stronger structural elements were used to ensure that the deformed primary lining would not invade the design space of the secondary lining. Especially for grade Vd-3 rock mass, a double-layer primary lining (Figure 15) was adopted to prevent large deformation of surrounding rock mass. In addition, the reversed deformation between the linings and the secondary lining parameters were also adaptable according to the ground conditions. The detailed parameters of the dynamically adaptive support system are listed in Table 3. Every 6 m (ten times the excavation step) during the excavation, a combination method with the transient electromagnetic method, ground penetrating radar, and advance

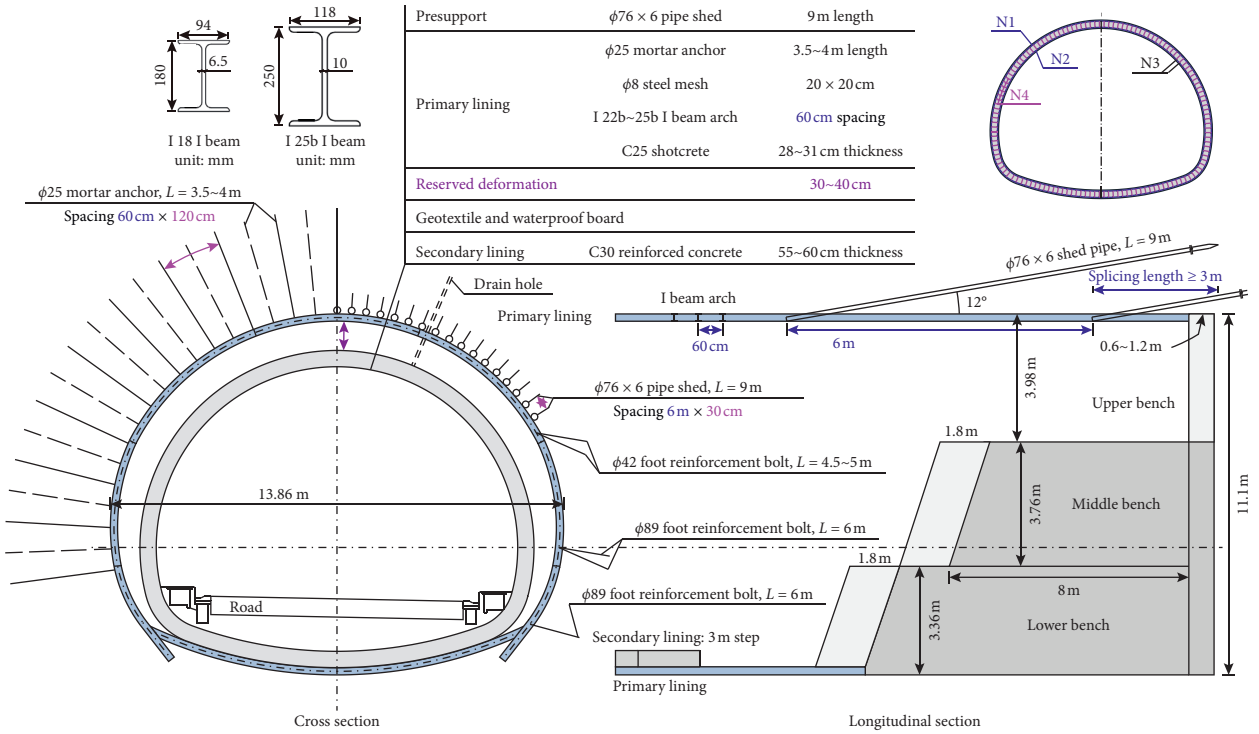

Figure 14: Schematic diagram of the dynamically adaptive support system in talus-like formations adopted in Tayi tunnel.

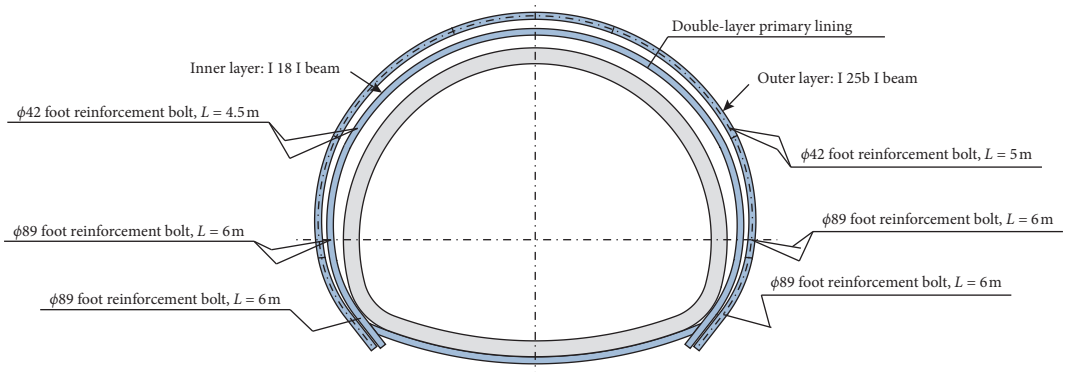

Figure 15: Configuration of foot reinforcement bolts in the double-layer primary lining for grade Vd-3 rock mass.

Table 3: Configuration of dynamically adaptive support system in talus-like formations in Tayi tunnel.

Supporting system		Vd-1	Vd-2	Vd-3
Presupport		φ76 × 6 pipe shed, 9 m length, 6 m × 30 cm spacing, splicing length ≥3 m		
Primary support	Mortal anchor	3.5 m length	φ25, 60 cm × 120 cm spacing, 4 m length	4 m length
	Steel mesh		φ8, 20 cm × 20 cm spacing	
	Steel arch	I 22b	60 cm spacing, I 25b	Double layer
	Shotcrete	28 cm	C25, 31 cm	Double layer
	Foot reinforcement bolt (each side)	Upper bench: φ42 × 2, 4.5 m length Middle bench: φ89 × 2, 6 m length Lower bench: φ89 × 1, 6 m length	Upper bench: φ42 × 2, 5 m length	Matched to steel arch
Reversed deformation		30~35 cm	35~40 cm	35~40 cm

Table 3: Continued.

Supporting system		Vd-1	Vd-2	Vd-3
Secondary support	Reinforced concrete	C30		
		50 cm	60 cm	60 cm
	Reinforcement	N1: φ22@20	N1: φ22@16.67	N1: φ22@16.67
		N2: φ22@20	N2: φ22@20	N2: φ22@20
		N3: φ14@30	N3: φ14@30	N3: φ14@30
		N4: φ8@30	N4: φ8@30	N4: φ8@30

Note: the primary support for Vd-3 is in the form of double-layer as shown in Figure 15. The unit for diameter of pipes, anchors, and steel bars is mm. The steel bars in N1, N2 and N3 are HRB 400 while the ones in N4 are HPB 300.

exploratory drilling was employed to detect the geological and hydrological conditions ahead of the excavation face to determine the subclass of the surrounding rock masses and the appropriate support parameters.

As stated above, the talus-like formations are sensitive to the excavation activities and the construction speed of Tayi tunnel has to be slowed down to reduce the deformation of surrounding rock mass and prevent the rock collapse. With the original support system (Figure 5) before August of 2020, the average excavation speed was less than 20 m per month in grade IV/V rock masses. The first-edition dynamically adaptive support system began to be used after August 2020 and the construction speed had been promoted to 30~40 m per month in grade V rock mass. Afterwards, the dynamically adaptive support system was improved in January 2021 as shown in Figures 14 and 15. As a result, the construction speed had been enhanced to 70~80 m per month in grade V rock mass (including the abovementioned grade Vd rock masses) and 160~180 m per month in grade IV rock mass. The maximum deformation of the primary lining was reduced to less than ~400 mm after the adoption of the dynamically adaptive support system.

5. Conclusion

This paper investigates the stability of Tayi tunnel passing through talus-like rock masses via site survey and in situ monitoring. In the project, the in situ monitoring items included the surrounding rock pressure on the primary lining, the stress of steel arches, and the deformation of the primary lining. The main conclusions are as follows.

(1) The deformation of the primary lining caused by the construction activities is larger than the deformation caused by surrounding rock creep in the talus-like ground. The construction activities have more impact on the closer sections than the farside sections.

(2) With the bench cut method, the surrounding rock pressure and the stress of steel arches increase rapidly soon after the excavation of the upper bench, then slightly drop down, and finally tend to be stable. The lower benches obviously release the surrounding rock pressure around the upper benches, inducing the decline of the surrounding rock pressure on the primary lining and the stress of steel arches.

(3) In terms of spatial distribution, the monitoring data usually has a characteristic of discreteness and nonuniformity along the tunnel periphery due to the uneven and asymmetrical contact between the surrounding rock mass and the primary lining which is inherently dominated by the uneven excavation space caused by complex formations of talus-like rock masses.

(4) It is suggested that the deformation of the surrounding rock masses should be emphatically disposed during the tunnel excavation in the talus-like ground. Termly advanced detection, flexible forepoling, timely closure of primary lining, and well-timed installation of secondary lining are recommended measures to reduce the deformation of the talus-like rock masses.

(5) A dynamically adaptive support system was implemented to strengthen the bearing capacity of the lining system according to the geological conditions of talus-like formations. After such treatment, the deformation of the primary lining has been well controlled and the construction speed has been considerably enhanced.

Data Availability

The data used to support the findings of this study are included within the article.

Conflicts of Interest

The authors declare that they have no conflicts of interest.

Acknowledgments

The research was supported by the National Natural Science Foundation of China (Grant no. 52008307) and POWERCHINA Roadbridge Group Co., Ltd. (Grant no. HHZ-JGY-FW-03).

References

[1] Q. Wang, X. Xie, and I. Shahrour, "Deep learning model for shield tunneling advance rate prediction in mixed ground condition considering past operations," *IEEE Access*, vol. 8, pp. 215310–215326, 2020.

[2] Z. Chen, C. He, G. Xu, G. Ma, and D. Wu, "A case study on the asymmetric deformation characteristics and mechanical behavior of deep-buried tunnel in phyllite," *Rock Mechanics and Rock Engineering*, vol. 52, no. 11, pp. 4527–4545, 2019.

[3] J. Liu, J. Wei, H. Hu, J. Wu, S. Sun, and D. P. Kanungo, "Research on the engineering geological conditions and stability evaluation of the B2 talus slide at the jin'an bridge hydropower station, China," *Bulletin of Engineering Geology and the Environment*, vol. 77, no. 1, pp. 105–125, 2018.

[4] H. Obanawa and Y. Matsukura, "Mathematical modeling of talus development," *Computers & Geosciences*, vol. 32, no. 9, pp. 1461–1478, 2006.

[5] H. Xing, L. Liu, and Y. Luo, "Water-induced changes in mechanical parameters of soil-rock mixture and their effect on talus slope stability," *Geomechanics and engineering*, vol. 18, no. 4, pp. 353–362, 2019.

[6] X. Li, Q. L. Liao, and J. M. He, "In situ tests and a stochastic structural model of rock and soil aggregate in the three gorges reservoir area, China," *International Journal of Rock Mechanics and Mining Sciences*, vol. 41, no. 3, pp. 494–499, 2004.

[7] D. Cen, D. Huang, and F. Ren, "Shear deformation and strength of the interphase between the soil-rock mixture and the benched bedrock slope surface," *Acta Geotechnica*, vol. 12, no. 2, pp. 391–413, 2017.

[8] X. Sun, X. Li, B. Zheng, J. He, and T. Mao, "Study on the progressive fracturing in soil and rock mixture under uniaxial compression conditions by CT scanning," *Engineering Geology*, vol. 279, no. 4, Article ID 105884, 2020.

[9] H. Dong, B. Peng, Q.-F. Gao, Y. Hu, and X. Jiang, "Study of hidden factors affecting the mechanical behavior of soil-rock mixtures based on abstraction idea," *Acta Geotechnica*, vol. 16, no. 2, pp. 595–611, 2021.

[10] W.-J. Xu and H.-Y. Zhang, "Research on the effect of rock content and sample size on the strength behavior of soil-rock mixture," *Bulletin of Engineering Geology and the Environment*, vol. 80, no. 3, pp. 2715–2726, 2021.

[11] N. Coli, P. Berry, and D. Boldini, "In situ non-conventional shear tests for the mechanical characterisation of a bimrock," *International Journal of Rock Mechanics and Mining Sciences*, vol. 48, no. 1, pp. 95–102, 2011.

[12] N. Coli, P. Berry, D. Boldini, and R. Bruno, "The contribution of geostatistics to the characterisation of some bimrock properties," *Engineering Geology*, vol. 137-138, pp. 53–63, 2012.

[13] W. J. Xu, X. Qiang, and R. L. Hu, "Study on the shear strength of soil–rock mixture by large scale direct shear test," *International Journal of Rock Mechanics and Mining Sciences*, vol. 48, no. 8, pp. 1235–1247, 2011.

[14] A. Kalender, H. Sonmez, E. Medley, C. Tunusluoglu, and K. E. Kasapoglu, "An approach to predicting the overall strengths of unwelded bimrocks and bimsoils," *Engineering Geology*, vol. 183, pp. 65–79, 2014.

[15] M. Afifipour and P. Moarefvand, "Mechanical behavior of bimrocks having high rock block proportion," *International Journal of Rock Mechanics and Mining Sciences*, vol. 65, pp. 40–48, 2014.

[16] M. Tsesarsky, M. Hazan, and E. Gal, "Estimating the elastic moduli and isotropy of block in matrix (bim) rocks by computational homogenization," *Engineering Geology*, vol. 200, pp. 58–65, 2016.

[17] W.-J. Xu, L.-M. Hu, and W. Gao, "Random generation of the meso-structure of a soil-rock mixture and its application in the study of the mechanical behavior in a landslide dam," *International Journal of Rock Mechanics and Mining Sciences*, vol. 86, pp. 166–178, 2016.

[18] Q. X. Meng, H. L. Wang, W. Y. Xu, and M. Cai, "A numerical homogenization study of the elastic property of a soil-rock mixture using random mesostructure generation," *Computers and Geotechnics*, vol. 98, pp. 48–57, 2018.

[19] E. Khorasani, M. Amini, M. F. Hossaini, and E. Medley, "Statistical analysis of bimslope stability using physical and numerical models," *Engineering Geology*, vol. 254, pp. 13–24, 2019.

[20] The National Standards Compilation Group of People's Republic of China, *GB/T 50128-2014 Standard for Engineering Classification of Rock Masses*, China Planning Press, Beijing, China, 2014.

[21] Chongqing Communications Technology Research and Design Institute, *JTG D70-2010, Code for Design of Road Tunnel*, China Communications Press, Beijing, China, 2010.

[22] H. Sonmez, E. Tuncay, and C. Gokceoglu, "Models to predict the uniaxial compressive strength and the modulus of elasticity for ankara agglomerate," *International Journal of Rock Mechanics and Mining Sciences*, vol. 41, no. 5, pp. 717–729, 2004.

[23] S. Sun, P. Xu, J. Wu et al., "Strength parameter identification and application of soil-rock mixture for steep-walled talus slopes in southwestern China," *Bulletin of Engineering Geology and the Environment*, vol. 73, no. 1, pp. 123–140, 2014.

[24] Z.-L. Zhang, W.-J. Xu, W. Xia, and H.-Y. Zhang, "Large-scale in-situ test for mechanical characterization of soil-rock mixture used in an embankment dam," *International Journal of Rock Mechanics and Mining Sciences*, vol. 86, pp. 317–322, 2016.

[25] P. F. Li, S. M. Tian, Y. Zhao, Y. Q. Zhu, and S. D. Wang, "In-situ monitoring study of mechanical characteristics of primary lining in weak rock tunnel with high geostress," *Chinese Journal of Rock Mechanics and Engineering*, vol. 32, no. Supp. 2, pp. 3509–3519, 2013, in Chinese.

[26] Q. Fang, W. Su, D. L. Zhang, and F. C. Yu, "Tunnel deformation characteristics based on on-site monitoring data," *Chinese Journal of Rock Mechanics and Engineering*, vol. 35, no. 9, pp. 1884–1897, 2016, in Chinese.

[27] X. L. Wang, J. X. Lai, R. S. Garnes, and Y. B. Luo, "Support system for tunnelling in squeezing ground of qingling-daba mountainous area: a case study from soft rock tunnels," *Advances in Civil Engineering*, vol. 2019, Article ID 8682535, 2019.

[28] J. X. Chen, Z. L. Xu, Y. B. Luo, J. K. Song, W. W. Liu, and F. F. Dong, "Application of the upper-bench CD method in super large-span and shallow tunnel: a case study of letuan tunnel," *Advances in Civil Engineering*, vol. 2020, Article ID 8826232, 2020.

[29] Q. G. Liang, J. Fang, and P. He, "Analysis on tunnel surrounding rock pressure characteristics based on field measured statistics," *Chinese Journal of Underground Space and Engineering*, vol. 16, no. 2, pp. 555–566, 2020, in Chinese.

[30] Q. Hong, H. Lai, Y. Liu, X. Ma, and J. Xie, "Deformation control method of a large cross-section tunnel overlaid by a soft-plastic loess layer: a case study," *Bulletin of Engineering Geology and the Environment*, vol. 80, no. 6, pp. 4717–4730, 2021.

[31] Z. Chen, C. He, G. Xu, G. Ma, and W. Yang, "Supporting mechanism and mechanical behavior of a double primary support method for tunnels in broken phyllite under high geo-stress: a case study," *Bulletin of Engineering Geology and the Environment*, vol. 78, no. 7, pp. 5253–5267, 2019.

[32] G. Xu, C. He, J. Wang, and Z. Chen, "Study on the mechanical behavior of a secondary tunnel lining with a yielding layer in transversely isotropic rock stratum," *Rock Mechanics and Rock Engineering*, vol. 53, no. 7, pp. 2957–2979, 2020.

[33] X. Sun, C. Zhao, Z. Tao, H. Kang, and M. He, "Failure mechanism and control technology of large deformation for muzhailing tunnel in stratified rock masses," *Bulletin of Engineering Geology and the Environment*, vol. 80, no. 6, pp. 4731–4750, 2021.